Pattern recognition approaches for the detection of alteration and degradation phenomena in hyperspectral and UAV multispectral imagery: the case study of a historical masonry water bridge

Alessandra Spadaro [1], Francesca Matrone [1], Andrea Maria Lingua [1], Ramin Rashidi Alavijeh [1]

[1] Geomatics Lab, Department of Environment, Land and Infrastructure Engineering, Politecnico di Torino, Corso Duca degli Abruzzi 24, 10129 Turin, Italy – (alessandra.spadaro, francesca.matrone, andrea.lingua, ramin.rashidi)@polito.it

Keywords: Hyperspectral imaging, Multispectral imagery, Decay mapping, UAV, OBIA, Machine Learning.

Abstract

Historical masonry hydraulic infrastructures are affected by complex degradation processes, including vegetation growth, moisture-related anomalies, and salt efflorescence, whose detection requires non-invasive, repeatable, and scalable diagnostic approaches. This study proposes a multi-scale workflow for detecting and classifying degradation phenomena affecting the Cavour Canal water bridge, a nineteenth-century masonry structure in northern Italy. The methodology combines UAV-based multispectral orthophotos and close-range hyperspectral imagery within a common Object-Based Image Analysis (OBIA) framework. The multispectral workflow was designed for façade-scale screening, whereas the hyperspectral workflow was used to support the detailed characterisation of selected sectors through detailed spectral characterisation. Multiple supervised classifiers, including Support Vector Machine (SVM), k-Nearest Neighbours (kNN), Decision Tree (DT), Random Trees (RT), and Naïve Bayes (NB), were tested on both datasets. The results show that the multispectral workflow is effective for identifying vegetation and broad water-related anomalies, with kNN providing the best overall performance, while the hyperspectral workflow improves the discrimination of subtle surface alterations, particularly efflorescence, with SVM yielding the most stable results across the tested configurations. Overall, the proposed methodology demonstrates the value of a hierarchical multispectral and hyperspectral workflow for non-invasive degradation mapping of historical masonry hydraulic infrastructures.

1. Introduction

The preservation of historical masonry infrastructures, such as water bridges, represents a critical challenge for both cultural heritage conservation and structural safety. These constructions embody significant technological and engineering achievements of the 19th century and continue to play a functional role in contemporary water management systems (Baratti, 1997).

However, prolonged exposure to environmental factors, including moisture fluctuations, biological colonization, and weathering, leads to progressive material degradation, which can compromise both their structural integrity and cultural value. Traditional inspection methods, primarily based on visual surveys and manual mapping, are often limited in their ability to detect early-stage degradation phenomena and to provide quantitative, repeatable assessments. In recent years, advances in geomatics and remote sensing have enabled the development of non-invasive diagnostic approaches, supporting more efficient and data-driven conservation strategies. In particular, multispectral and hyperspectral imaging techniques have demonstrated significant potential in identifying material properties and detecting alteration processes that are not visible in the standard optical domain (Del Pozo et al., 2016; Markiewicz et al., 2019). Multispectral imagery, especially when acquired via Unmanned Aerial Vehicles (UAVs), allows for rapid and large-scale documentation of surfaces, facilitating the identification of macroscopic degradation patterns such as vegetation growth and moisture-related anomalies. Conversely, hyperspectral imaging provides high spectral resolution data, enabling detailed material discrimination and the detection of subtle chemical and physical alterations, such as efflorescence and early-stage decay. The integration of these complementary data sources is therefore particularly promising for heritage diagnostics, as it combines the synoptic capacity of UAV-based surveys with the material-sensitive detail of close-range spectral analysis.

1.1 State of the art

The application of remote sensing techniques to cultural heritage diagnostics has significantly expanded over the past decade, particularly with the adoption of multispectral and hyperspectral imaging for material characterization and degradation mapping (Hemmleb et al., 2006; Chun et al., 2015; Adamopoulos, 2021). Hyperspectral data have been widely used to detect mineralogical and chemical changes in stone materials, supporting the identification of weathering processes and biological growth (Blanco et al., 2012; Matoušková et al., 2024). Similarly, UAV-based multispectral systems have enabled efficient acquisition of high-resolution data for large and complex structures, improving accessibility and reducing operational costs (Huang et al., 2022). In parallel, machine learning approaches have been increasingly employed to automate the classification of surface materials and degradation patterns. Both pixel-based and object-based image analysis (OBIA) methods have been explored, with OBIA showing advantages in incorporating spatial context and reducing noise effects in high-resolution imagery (Li et al., 2019; Jiménez-Jiménez et al., 2020; Belcore et al., 2021). Supervised classification algorithms such as Support Vector Machines (SVM), k-Nearest Neighbors (kNN), Decision Trees, and ensemble methods have demonstrated strong performance in remote sensing classification tasks, including heritage applications (Nick et al., 2015; Ahmadian et al., 2024).

Despite these advancements, several challenges remain. First, most studies focus on single-sensor datasets, limiting the ability to capture degradation phenomena across multiple spatial and spectral scales. Second, the integration of multispectral and hyperspectral data is still relatively underexplored, particularly in the context of cultural heritage monitoring. Third, the transferability and robustness of classification models across different scenes and acquisition conditions require further investigation (Gao et al., 2018; Kang et al., 2025). These

https://doi.org/10.5194/isprs-archives-XLIX-B2-2026-893-2026

limitations are especially critical in historical masonry structures, where material heterogeneity, weathering patterns, and moisture-related processes often coexist and generate spectrally ambiguous responses.

1.2 Research objectives and contributions

This study aims to develop and validate a multi-scale, semi-automatic workflow for the detection and classification of degradation phenomena affecting historical masonry structures. The proposed approach integrates UAV-based multispectral imagery and close-range hyperspectral data to leverage their complementary characteristics in terms of spatial and spectral resolution. The methodology combines photogrammetric processing, hyperspectral preprocessing, OBIA, and supervised machine learning classification to produce detailed and consistent degradation maps. The approach is tested on a representative case study of a 19th-century masonry water bridge, affected by multiple deterioration processes, including efflorescence, moisture infiltration, and biological growth.

The main contributions of this work can be summarized as follows:

- Development of an integrated workflow combining multispectral and hyperspectral data for multi-scale degradation mapping;
- Implementation and comparison of multiple supervised classification algorithms within an OBIA framework;
- Evaluation of classification performance using quantitative accuracy metrics;
- Assessment of the potential of multi-sensor hierarchical integration of multispectral and hyperspectral workflow for supporting non-invasive, repeatable monitoring of historical infrastructures.

The proposed framework is intended not only to improve degradation detection, but also to support conservation-oriented decision making by linking large-scale screening, detailed material interpretation, and repeatable monitoring strategies.

2. Study area

The study focuses on a historical masonry water bridge belonging to the Cavour Canal system, one of the most significant hydraulic engineering infrastructures constructed in Italy during the 19th century. The Cavour Canal, built between 1863 and 1866, was designed to support irrigation over an extensive agricultural area of approximately 200,000 hectares, with a discharge capacity of about 110 m^3/s and a total length of approximately 82 km (Baratti, 1997).

The selected case study is the Ponte Canale Cavour over the Dora Baltea River (Figure 1), located near the municipality of Saluggia in Vercelli, north-western Italy. This structure represents the first and one of the most important hydraulic crossings within the canal system, completed in 1864. The bridge is characterized by a monumental masonry architecture, consisting of approximately 193.6 m in length, with nine masonry arches supported by eight piers and two abutments. The structural system is primarily composed of fired clay bricks, with localized use of stone elements (e.g., granite slabs) in the lower portions of the piers to enhance resistance to hydraulic erosion.

The material composition reflects typical construction practices of 19th-century hydraulic infrastructures, where brick masonry was widely used due to its mechanical performance and availability. However, the intrinsic porosity of these materials makes them particularly vulnerable to environmental stressors, including moisture ingress and salt crystallization processes.

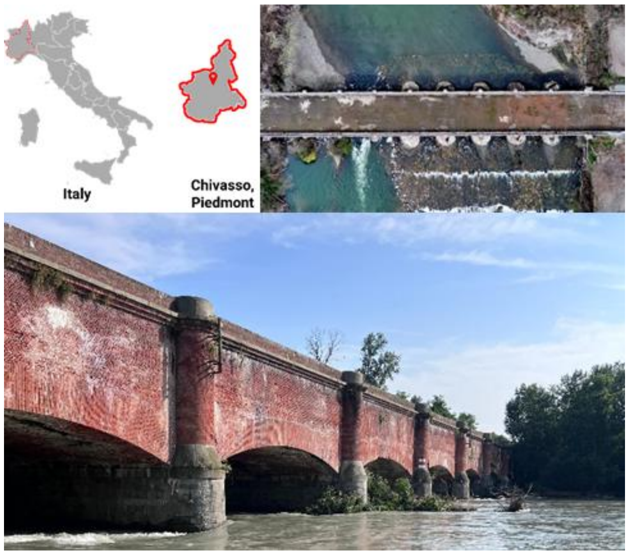

Figure 1. The Cavour Canal water bridge over the Dora Baltea River (Saluggia, Italy), a 19th-century masonry hydraulic structure characterized by a multi-arch configuration and a continuous water conveyance system.

The bridge is situated within the alluvial plain of the Dora Baltea River, in a geomorphological and environmental context characterized by significant hydrological variability. Seasonal fluctuations in river discharge, driven by precipitation and snowmelt, induce recurrent wetting–drying cycles that strongly influence the conservation state of the masonry structure. Additionally, the surrounding landscape is dominated by intensively cultivated agricultural areas, which contribute to high humidity levels and biological activity in proximity to the structure. Despite restoration interventions carried out in recent decades, the bridge is currently affected by several degradation phenomena. Field observations and preliminary inspections have identified multiple forms of decay, including:

- *Efflorescence*, associated with salt crystallization processes;
- *Surface erosion*, linked to prolonged exposure to atmospheric agents;
- *Moisture infiltration*, particularly evident in the piers and lower sections of the structure;
- *Biological growth*, such as vegetation and microorganisms, which contribute to material deterioration.

These degradation processes are spatially heterogeneous and often occur simultaneously, making their detection and classification particularly challenging. Their progression is influenced by the interaction between environmental conditions, material properties, and structural characteristics, requiring diagnostic approaches capable of capturing both large-scale patterns and fine-scale material variations.

The study area offers a representative testbed for evaluating advanced geomatics-based methodologies due to the presence of multi-scale degradation phenomena, the complex geometry of the structure, the interaction between environmental dynamics and material decay, and the need for non-invasive and repeatable monitoring techniques. Moreover, the bridge still performs an active hydraulic function, which increases the practical relevance of implementing fast, repeatable, and scalable diagnostic procedures. Figures 2 illustrates the main degradation phenomena affecting the masonry surfaces.

Figure 2. Examples of degradation phenomena affecting the masonry structure, including moisture infiltration and biological growth, contribute to material decay and structural weakening.

3. Data and methods

This section presents the methodological framework adopted to integrate UAV-based multispectral imagery and close-range hyperspectral data for degradation mapping. The workflow was designed to combine façade-scale coverage with detailed material discrimination through a sequence of acquisition, preprocessing, object-based segmentation, supervised classification, and accuracy assessment steps.

3.1 Overall workflow

The proposed methodology is based on a multi-scale and multi-sensor workflow designed to integrate UAV-based multispectral imagery and close-range hyperspectral data for the detection and classification of degradation phenomena affecting historical masonry structures. The workflow consists of the following main steps:

- Data acquisition and photogrammetric process of multispectral UAV data;
- Data acquisition, geometric registration, and radiometric calibration of hyperspectral imagery;
- Object-Based Image Analysis (OBIA);
- Supervised classification;
- Accuracy assessment.

As shown in Figure 3, the proposed methodology integrates two sensor-specific workflows within a common object-based analytical framework. The multispectral workflow provides synoptic information at façade scale, while the hyperspectral workflow refines the interpretation of selected sectors through more detailed spectral characterisation. The integration of multi-resolution datasets enables the combined analysis of large-scale surface patterns and fine-scale material characteristics.

3.2 Multispectral data acquisition and processing

Multispectral data were acquired using a DJI Mavic 3 Multispectral UAV platform, equipped with an integrated RTK module and a multi-camera system including an RGB sensor and four monochromatic sensors operating in the green, red, red-edge (RE), and near-infrared (NIR) spectral bands.

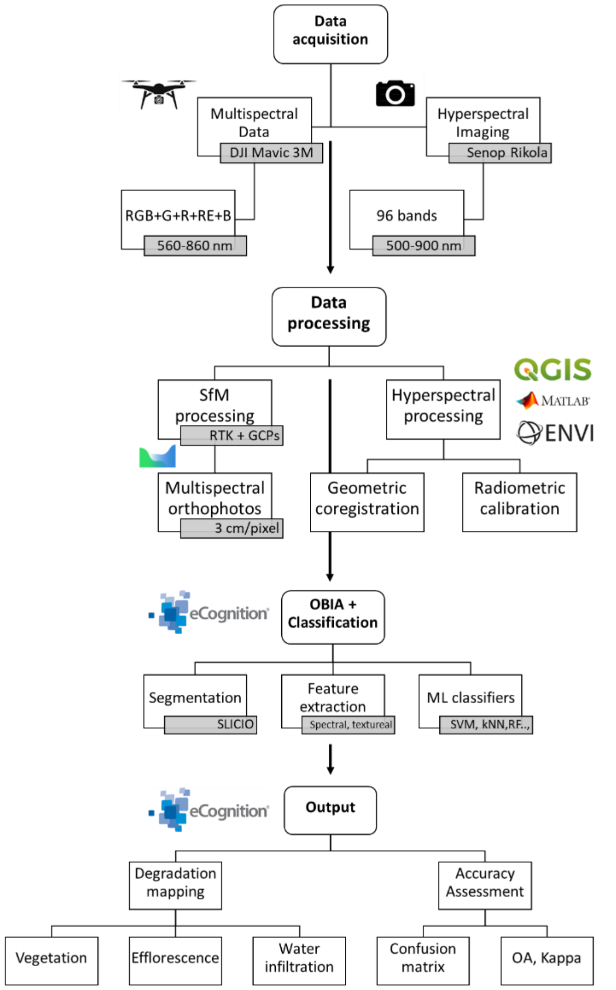

Figure 3. Workflow of the proposed multi-scale and multi-sensor methodology integrating UAV-based multispectral and close-range hyperspectral data.

The acquisition campaign (Figure 4a), comprising approximately 2500 images per sensor, was designed to ensure complete coverage of the bridge façades and structural elements, including nadir and oblique images, with particular attention to areas affected by visible degradation phenomena, such as moisture infiltration and biological growth.

The survey yielded an original GSD of 2.5 mm per pixel. For the subsequent object-based analysis, the multispectral orthophotos were resampled to approximately 3 cm in order to reduce noise and computational burden while preserving the spatial scale of the target degradation patterns at façade level.

A dedicated topographic network was established to ensure accurate georeferencing of the dataset. Four control vertices were first acquired using GNSS receivers in static mode, with acquisition sessions of approximately one hour to guarantee high positional accuracy. These points were used as a reference for the definition of the global reference system. Subsequently, a set of Ground Control Points (GCPs) was acquired along the bridge façades using a Total Station, including both artificial markers and clearly identifiable natural features, with a density of eight GCPs for each bridge arch, thus ensuring a robust and well-distributed georeferencing of the photogrammetric model.
Photogrammetric processing was performed in Agisoft Metashape v2.2.3 following a standard Structure-from-Motion (SfM) workflow, including image alignment and sparse point

cloud generation (Figure 4b), georeferencing based on RTK data and GCPs, dense point cloud reconstruction, and the generation of RGB and multispectral orthophotos. The integration of onboard RTK positioning with ground-based control points allowed for improved geometric accuracy and consistency of the final products. The final photogrammetric solution achieved a 3D RMSE of 1.3 and 1.8 cm RMSE on Ground Control Points (GCPs) and Check Points (CPs), respectively. The resulting multispectral orthophotos (Figure 4c) provide a geometrically consistent basis for façade-scale analysis and for the detection of macro-scale degradation patterns, particularly vegetation growth and moisture-affected areas. No absolute radiometric calibration was applied to the multispectral dataset; therefore, the orthophotos were used as spectrally consistent relative products for object-based classification.

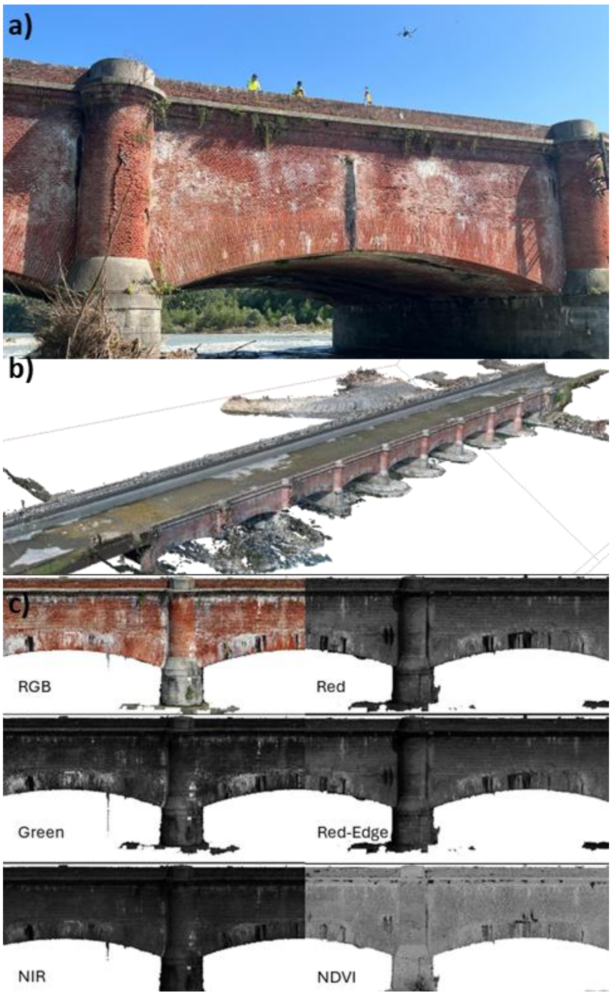

Figure 4. Multispectral data acquisition and processing: (a) UAV survey using DJI Mavic 3M, (b) reconstructed point cloud and flight geometry, and (c) multispectral orthophoto used for large-scale degradation mapping.

3.3 Hyperspectral data acquisition and processing

Hyperspectral data were acquired using a Senop Rikola hyperspectral frame camera, operating in the visible and near-infrared spectral range (500–900 nm) and providing 96 narrow and contiguous spectral bands with high spectral resolution (Figure 5). The sensor configuration enables detailed spectral characterization of materials, making it particularly suitable for detecting subtle surface alterations in masonry structures.

Data acquisition was performed from a close-range configuration, with the camera mounted on a tripod and positioned approximately orthogonally to the bridge façades. A dark reference measurement was acquired in situ to reduce sensor-related noise and improve data quality.

The preprocessing workflow focused primarily on ensuring geometric consistency across spectral bands and improving the robustness of the dataset for classification. Band-to-band co-registration was performed using a feature-based approach implemented in MATLAB, relying on ORB descriptors to estimate projective transformations between each band and a selected reference band. This step ensured pixel-level alignment across all spectral channels, which is essential for reliable spectral analysis. An alternative co-registration approach was tested in QGIS using the AROSICS plugin; however, the MATLAB-based workflow provided more stable results, particularly in low-texture regions. Radiometric calibration was performed to convert raw digital numbers into physically meaningful reflectance-related values, enabling consistent comparison of spectral responses across the dataset. Following calibration, additional preprocessing steps were applied to improve data quality, including the masking of shadowed areas, vegetation occlusions, and low-quality regions. These operations reduced noise and minimized the influence of irrelevant features on subsequent analysis.

The resulting hyperspectral cubes provide a geometrically and radiometrically consistent dataset, suitable for advanced spectral–spatial analysis and object-based classification.

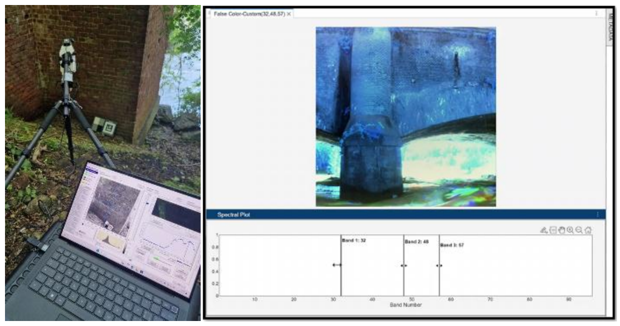

Figure 5. Hyperspectral close-range data acquisition using the Senop Rikola camera.

3.4 Object-Based Image Analysis (OBIA)

Both multispectral orthophotos and hyperspectral datasets were processed using an OBIA approach implemented in eCognition Developer v10.1.

A multiresolution segmentation algorithm was applied to group pixels into meaningful image objects based on spectral homogeneity and spatial proximity. The segmentation parameters were iteratively adjusted to achieve a balance between preserving material boundaries and reducing intra-class variability. This step is particularly important in complex masonry surfaces, where spectral variability within the same material can be high due to environmental and degradation effects. The use of OBIA enabled the integration of spectral, spatial, and geometric information, providing a more robust framework compared to pixel-based approaches for the classification of heterogeneous surfaces.

3.5 Feature extraction and supervised classification

Following segmentation, each image object was described through a combination of features:

- *spectral features* (mean values of green, red, NIR, and red-edge bands);
- *spectral indices*, including NDVI and NDWI;
- *geometric features*, such as compactness, asymmetry, and length-to-width ratio;
- *textural features*, derived from Gray Level Co-occurrence Matrix (GLCM).

Supervised classification was then performed using multiple machine learning algorithms, including Support Vector Machine (SVM), k-Nearest Neighbours (kNN), Decision Tree (DT), Random Trees (RT), and Naïve Bayes (NB). The classification scheme was designed to discriminate among three degradation-related classes relevant to the study: vegetation, water-related anomalies, and efflorescence. Testing multiple classifiers enabled a comparative evaluation of their performance and robustness with respect to feature selection, segmentation scale, and dataset characteristics.

3.6 Accuracy assessment

Classification performance was evaluated through a quantitative framework based on confusion matrices, Overall Accuracy (OA), Produce and Kappa Index of Agreement (KIA). Training and validation datasets were defined as independent spatial subsets, following a 70:30 ratio (train/validation and test), in order to ensure an unbiased assessment of model performance. In addition to global accuracy measures, class-wise Producer's and User's Accuracies were analysed to better interpret the reliability of the degradation-related classes. This was particularly important for water-related anomalies and efflorescence, whose spectral responses may overlap with other surface conditions.

4. Results

This section presents the results obtained from the multispectral and hyperspectral workflows for the classification of degradation-related patterns affecting the masonry surfaces of the Cavour Canal water bridge. The two sensor-specific workflows are first reported separately in order to highlight their respective performance, and are then compared to assess their complementary contribution to multi-scale degradation mapping.

4.1 Multispectral workflow results

The multispectral workflow enabled façade-scale classification of the bridge surfaces and proved effective for the identification of the three degradation-related classes considered in this study (vegetation, water-related anomalies, and efflorescence).

As summarised in Table 1, classifier performance differed markedly across the tested configurations. kNN achieved the best overall result, with an Overall Accuracy (OA) of 91.5% and a Kappa Index of Agreement (KIA) of 0.806. RT and NB also yielded strong results, with OA values of 87.4% and 87.2%, respectively, while DT reached 81.3%. By contrast, SVM showed substantially lower performance than all the other classifiers, with OA and KIA values close to zero. Under the tested configuration, it did not provide reliable results for the multispectral dataset.

The RGB-only kNN baseline, introduced to assess the contribution of multispectral information beyond the visible range, achieved an OA of 89.2% and a KIA of 0.752. Compared with the full multispectral configuration, this result indicates a moderate but consistent improvement when near-infrared and red-edge information are included in the feature space.

At class level, vegetation showed generally good separability. NB provided the best class-specific result, with PA = 91.8% and UA = 97.3%, while kNN also performed well (PA = 73.0%, UA = 93.2%). RT and DT yielded lower but still satisfactory values. In comparison, the RGB-only kNN baseline produced lower accuracies for vegetation, confirming the added value of multispectral information for this class.

Water-related anomalies also showed relatively high separability, although with greater variability among classifiers. NB achieved the best result for this class (PA = 95.9%, UA = 94.9%), followed by kNN (PA = 87.9%, UA = 97.6%) and RT (PA = 80.1%, UA = 93.0%). DT produced lower accuracies, while SVM again failed to produce meaningful discrimination. The RGB-only kNN baseline achieved lower values than the full multispectral configuration, particularly in terms of PA.

Efflorescence was classified with high accuracy by several classifiers. kNN yielded the best balance (PA = 94.2%, UA = 98.2%), closely followed by RT (PA = 90.1%, UA = 98.6%). NB and DT also achieved high UA values, although with slightly lower PA. In this case, the difference between the full multispectral configuration and the RGB-only kNN baseline was more limited than for vegetation and water-related anomalies.

Representative classification outputs are shown in Figure 6. Overall, the multispectral workflow provided a robust basis for rapid façade-scale screening, with kNN emerging as the best-performing classifier in terms of overall accuracy.

Classifier	**OA (%)**	**KIA (-)**	**Vegetation PA/UA (%)**	**Water PA/UA (%)**	**Efflorescence PA/UA (%)**
kNN	91.5	0.81	73.0/93.2	87.9/97.6	94.2/98.2
RGB kNN	89.2	0.75	61.0/82.6	80.5/91.3	94.0/97.8
RT	87.4	0.73	79.6/90.4	80.1/93.0	90.1/98.6
NB	87.2	0.74	91.8/97.3	95.9/94.9	84.5/99.4
DT	81.3	0.63	78.0/96.9	72.9/92.9	83.8/98.8
SVM	1.7	0.01	17.3/10.5	1.0/8.5	0.5/88.9

Table 1. Multispectral classification results for the degradation-related classes.

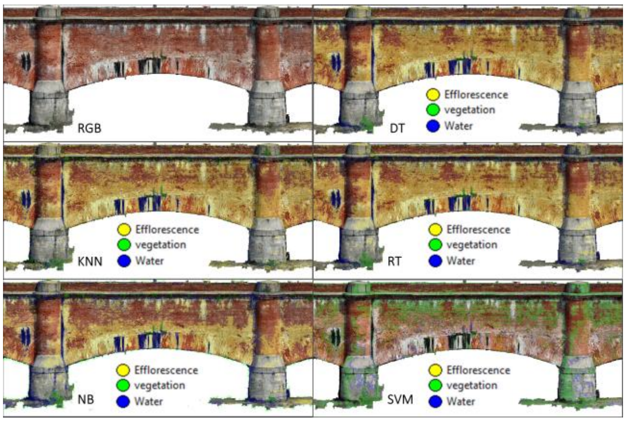

Figure 6. Multispectral classification outputs obtained from the object-based analysis of the UAV-derived orthophotos. The maps highlight the spatial distribution of vegetation, water-related anomalies, and efflorescence across the masonry surfaces.

4.2 Hyperspectral workflow results

The hyperspectral workflow was applied to selected sectors in order to refine the interpretation of degradation-related patterns through a more detailed spectral characterisation. Classification was performed on object-based segments derived from close-range hyperspectral imagery, and the influence of feature selection, segmentation scale, and scene configuration was also evaluated.

The results reported in Table 2 show that the hyperspectral workflow achieved high classification performance overall, although differences among classifiers remained evident. In Scene 1, SVM provided the highest OA and KIA values (OA = 89.8%, KIA = 0.8447), followed by NB (OA = 80.0%, KIA = 0.718), RT (OA = 78.6%, KIA = 0.699), kNN (OA = 77.6%, KIA = 0.665), and DT (OA = 65.9%, KIA = 0.540). In Scene 2, SVM again ranked first (OA = 84.6%, KIA = 0.786), closely followed by RT (OA = 84.2%, KIA = 0.779) and DT (OA = 83.4%, KIA = 0.768).

A refined configuration based on improved masking and sample selection further increased classification reliability. Under this setting, SVM achieved OA = 89.3% and KIA = 0.854, while NB reached OA = 86.5% and KIA = 0.812. As shown in Table 3, SVM provided the most balanced class-wise performance across the three degradation-related classes, with 79.9% / 100.0% for water-related anomalies, 89.9% / 87.8% for vegetation, and 89.2% / 91.4% for efflorescence, in terms of PA / UA. NB was particularly effective for efflorescence, reaching PA = 95.6% and UA = 90.9%, although its performance for water-related anomalies was less stable.

The experiments also showed that the classification outcome was influenced by feature composition and segmentation scale. The integration of spectral and geometric descriptors generally improved classification stability, whereas textural descriptors did not systematically enhance performance. In addition, overly fine segmentation increased intra-class variability, while overly coarse segmentation tended to merge distinct surface responses. The most reliable results were obtained at an intermediate segmentation level.

Representative outputs of the refined hyperspectral classification are shown in Figure 7. Overall, the hyperspectral workflow provided more detailed discrimination of subtle surface alterations than the multispectral workflow, particularly in relation to efflorescence.

Dataset / configuration	SVM OA / KIA	kNN OA / KIA	DT OA / KIA	RT OA / KIA	NB OA / KIA
Scene 1	89.8 / 0.8447	77.6 / 0.665	65.9 / 0.540	78.6 / 0.699	80.0 / 0.718
Refined Scene 1	89.3 / 0.854	81.1 / 0.744	75.7 / 0.673	71.6 / 0.617	86.5 / 0.812
Scene 2	84.6 / 0.786	80.5 / 0.730	83.4 / 0.768	84.2 / 0.779	79.5 / 0.710

Table 2. Summary of the hyperspectral classification results obtained on the analysed scenes.

Classifier	Water PA / UA (%)	Vegetation PA / UA (%)	Efflorescence PA / UA (%)
SVM	79.9 / 100.0	89.9 / 87.8	89.2 / 91.4
NB	62.7 / 100.0	93.4 / 78.7	95.6 / 90.9

Table 3. Class-wise accuracies for the refined Scene 1 hyperspectral classification configuration.

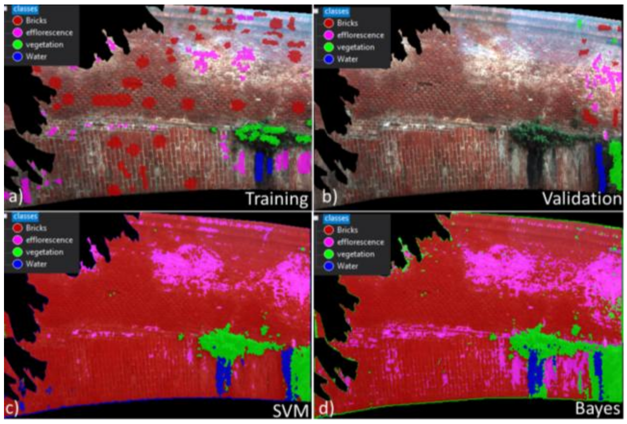

Figure 7. Representative hyperspectral classification results for the refined Scene 1 object-based configuration: (a) training dataset; (b) validation dataset; (c) SVM classification map; and (d) Naïve Bayes classification map.

4.3 Classifier comparison

Comparison of the two sensor-specific workflows revealed a clear difference in classifier behaviour. In the multispectral workflow, kNN achieved the best overall performance, while NB also yielded strong and consistent results for vegetation and water-related anomalies. In the hyperspectral workflow, by contrast, SVM produced the most stable and balanced classification across the tested configurations, with NB emerging as a competitive alternative in the refined setup.

The class of vegetation proved to be relatively stable across both workflows. Water-related anomalies were also identified effectively, although performance was more dependent on classifier choice. The most relevant difference concerned efflorescence: while this class was already well detected in the multispectral workflow, the hyperspectral workflow provided more reliable discrimination under the refined configuration.

The comparison between the full multispectral setup and the RGB-only kNN baseline further highlighted the contribution of multispectral information. The increase from OA = 89.2% to OA = 91.5%, and from KIA = 0.752 to KIA = 0.806, indicates that the inclusion of non-visible bands improved classification performance, especially for vegetation and water-related anomalies.

Taken together, these results show that the two workflows are not redundant, but provide complementary information at different scales. The multispectral workflow supports broad façade-scale screening, whereas the hyperspectral workflow refines the analysis of selected sectors where more detailed spectral discrimination is required.

4.4 Implications for multi-scale degradation mapping

Taken together, the results show that the two sensor-specific workflows are complementary rather than redundant. The multispectral workflow is effective for rapid façade-scale screening of vegetation, water-related anomalies, and sectors potentially affected by efflorescence, while providing broad spatial coverage and high operational efficiency.

The hyperspectral workflow addresses the main limitation of the multispectral workflow by improving the discrimination of subtle degradation patterns, especially efflorescence, through a more detailed spectral characterisation. In practical terms, this supports a hierarchical strategy: multispectral orthophotos can first identify priority areas across the whole structure, after which hyperspectral analysis can refine the diagnosis in selected sectors.

At the same time, the results highlight a relevant methodological limitation when dealing with real degradation processes, namely the co-occurrence of multiple phenomena on the same surface. In the current workflow, each object is assigned to a single class, whereas in practice vegetation may coexist with water-related anomalies, and efflorescence may develop in areas simultaneously affected by moisture. Such mixed conditions are difficult to represent within a single-label classification framework and may therefore lead to oversimplified thematic outputs. Examples of these situations are illustrated in Figure 8, where overlapping degradation patterns complicate the association and recognition of a single dominant class.

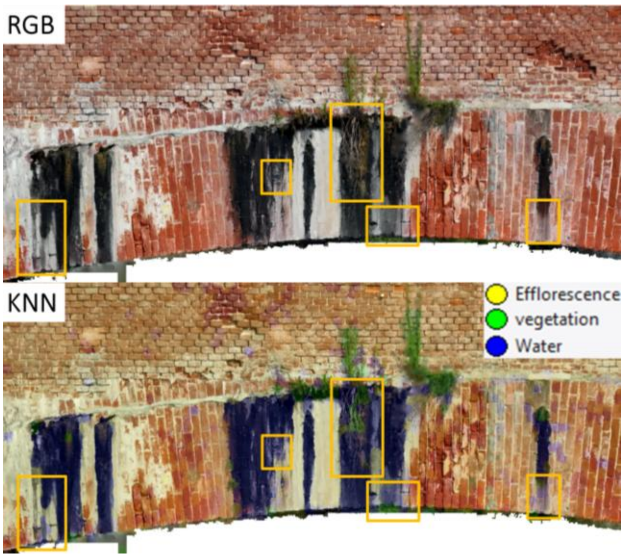

Figure 8. Examples of spatial coexistence of degradation-related phenomena on the masonry surfaces. The highlighted areas show cases in which vegetation, water-related anomalies, and efflorescence may visually overlap.

This aspect suggests that future developments should investigate multi-label or soft-classification strategies, together with object-refinement approaches capable of separating mixed degradation responses more effectively.

This multi-scale integration is particularly relevant for heritage monitoring, where both wide-area coverage and material-sensitive interpretation are required. The proposed workflow therefore provides a solid basis for repeatable degradation mapping and for future integration with maintenance-oriented digital models and decision-support systems.

5. Discussions and future works

The results highlight the value of integrating UAV-based multispectral orthophotos and close-range hyperspectral imagery within a common object-based workflow for the mapping of degradation-related patterns on historical masonry surfaces. The two sensor-specific workflows should not be regarded as alternative solutions, but as complementary components of a hierarchical diagnostic strategy.

The multispectral workflow proved effective for façade-scale screening, providing broad spatial coverage and satisfactory accuracy for vegetation, water-related anomalies, and, to a certain extent, efflorescence. The comparison with the RGB-only kNN baseline suggests that the inclusion of near-infrared and red-edge information improves class separability, particularly for vegetation and moisture-related surface responses. This makes the multispectral workflow well-suited to the rapid identification of priority areas requiring closer inspection.

A second relevant outcome concerns the sensor-dependent behaviour of the classifiers. In the multispectral workflow, kNN and NB produced the most reliable results, whereas in the hyperspectral workflow SVM provided the most stable and balanced performance. This difference suggests that classifier suitability depends on the structure of the feature space, including spectral dimensionality and class separability. In this context, the poor SVM performance observed in the multispectral workflow should be interpreted cautiously, as it is likely related to the specific dataset and tested configuration rather than to the classifier itself. A possible explanation is the combination of limited spectral dimensionality, partial overlap among degradation-related classes, and sensitivity to parameterisation.

The hyperspectral workflow proved particularly useful for the discrimination of subtle surface alterations, especially efflorescence. Its main contribution therefore lies less in broad screening capability than in the refined interpretation of diagnostically critical sectors. This reinforces the value of a multi-scale strategy in which multispectral data support initial screening and hyperspectral data are used for targeted refinement.

A relevant limitation concerns the representation of mixed degradation conditions. Real masonry surfaces often exhibit co-occurring processes, such as vegetation associated with water-related anomalies or efflorescence developing in moisture-affected areas. Since the present workflow assigns one dominant label to each object, the resulting maps should be interpreted primarily as representations of prevailing surface conditions rather than exhaustive descriptions of all concurrent processes.

Future work should therefore focus on improving the representation of mixed degradation patterns, testing the transferability of the multispectral and hyperspectral workflow under different acquisition conditions, and integrating the resulting maps into maintenance-oriented digital environments for repeatable heritage monitoring.

6. Conclusions

This study presented a multi-scale workflow for the detection and classification of degradation phenomena affecting a historical masonry water bridge, integrating UAV-based multispectral orthophotos and close-range hyperspectral imagery within a common object-based framework. The proposed approach combined acquisition, preprocessing, supervised classification, and quantitative assessment in order to evaluate the complementary contribution of the two sensor-specific workflows.

The results showed that the multispectral workflow is particularly effective for façade-scale screening. kNN achieved the best overall performance (OA = 91.5%, KIA = 0.806), while NB yielded strong results for vegetation and water-related anomalies, and RT proved effective for efflorescence. The comparison with the RGB-only kNN baseline further highlighted the added value of multispectral information beyond visible bands alone, especially for vegetation and water-related anomalies.

https://doi.org/10.5194/isprs-archives-XLIX-B2-2026-893-2026

The hyperspectral workflow provided a more detailed interpretation of subtle degradation patterns. SVM achieved the most stable performance across the analysed configurations, while NB emerged as a competitive alternative for efflorescence. These results suggest that the main contribution of hyperspectral imagery lies in its higher diagnostic specificity rather than in a simple increase in overall accuracy.

A further outcome of the study is the clear sensor-dependent behaviour of the classifiers. Multispectral data favoured kNN- and NB-based solutions, whereas hyperspectral data were more effectively handled by SVM. This suggests that classifier selection should be guided not only by accuracy values, but also by the structure of the feature space and by the specific diagnostic objective.

Overall, the study shows that the integration of multispectral and hyperspectral data can support a hierarchical degradation-mapping strategy, in which façade-scale screening is combined with localised, material-sensitive diagnosis. Future work should focus on strengthening the validation framework, improving the transferability of the multispectral and hyperspectral workflow, and exploring classification strategies better suited to mixed degradation conditions to integrate the resulting maps into maintenance-oriented digital monitoring systems.

Acknowledgments

This research was conducted within the RETURN Extended Partnership (PE0000005, SPOKE 6 – TS2) and the FAIR – Future Artificial Intelligence Research project (PE00000013), both funded by the European Union NextGenerationEU under the National Recovery and Resilience Plan (NRRP), Mission 4, Component 2, Investment 1.3. This manuscript reflects only the authors’ views and opinions, neither the European Union nor the European Commission can be considered responsible for them.
The authors would like to thank the *Associazione di Irrigazione Ovest Sesia* (AIOS) for the support during the field activities and access to the water bridge and the student team DIRECT from Politecnico di Torino supporting the in field acquisition phase.

References

Adamopoulos, E., 2021: Learning-based classification of multispectral images for deterioration mapping of historic structures. *Journal of Building Pathology and Rehabilitation*, 6(1), 41.

Ahmadian, V., Aval, S.B.B., Noori, M., Wang, T., Altabey, W.A., 2024: Comparative study of a newly proposed machine learning classification to detect damage occurrence in structures. *Engineering Applications of Artificial Intelligence*, 127, 107226.

Baratti, C., 1997: I Fontanili del Novarese. *Novara, Associazione Irrigazione Est Sesia, Stampa.*

Belcore, E., Di Pietra, V., Grasso, N., Piras, M., Tondolo, F., Savino, P., Polania, D.R., Osello, A., 2021: Towards a FOSS automatic classification of defects for bridges structural health monitoring. In: *Italian Conference on Geomatics and Geospatial Technologies,* pp. 298-312.

Blanco, F., Lopez-Mesas, M., Serranti, S., Bonifazi, G., Havel, J., Valiente, M., 2012: Hyperspectral imaging based method for fast characterization of kidney stone types. *Journal of Biomedical Optics*, 17(7), 076027-076027.
Chun, Y.G., Lee, M.S., Kim, Y.R., Lee, M.H., Choi, M.J., Choi, K.H., 2015: Utilization of hyperspectral image analysis for monitoring of stone cultural heritages. *Journal of Conservation Science*, 31(4), 395-402.

Del Pozo, S., Sánchez-Aparicio, L.J., Rodríguez-Gonzálvez, P., Herrero-Pascual, J., Muñoz-Nieto, A., González-Aguilera, D., Hernández-López, D., 2016: Multispectral imaging: Fundamentals, principles and methods of damage assessment in constructions. *Non-Destructive Techniques for the Evaluation of Structures and Infrastructure*, 11, 139.

Gao, Y., Mosalam, K.M., 2018: Deep transfer learning for image-based structural damage recognition. *Computer-Aided Civil and Infrastructure Engineering*, 33(9), 748-768.

Hemmleb, M., Weritz, F., Schiemenz, A., Grote, A., Maierhofer, C., 2006: Multi-spectral data acquisition and processing techniques for damage detection on building surfaces. *Image Engineering and Vision Metrology*, Dresden, Germany.

Huang, X., Wang, P., Zhang, S., Zhao, X., Zhang, Y., 2022: Structural health monitoring and material safety with multispectral technique: A review. *Journal of Safety Science and Resilience*, 3(1), 48-60.

Jiménez-Jiménez, S.I., Ojeda-Bustamante, W., Ontiveros-Capurata, R.E., Marcial-Pablo, M.D.J., 2020: Rapid urban flood damage assessment using high resolution remote sensing data and an object-based approach. *Geomatics, Natural Hazards and Risk*, 11(1), 906-927.

Kang, D.K., Olsen, M.J., Fischer, E., Jung, J., Adams, J.A., 2025: Deep learning transferability across disaster types for UAS imagery based building damage assessment. *Discover Civil Engineering*, 2(1), 1-24.

Li, S., Zhao, X., Zhou, G., 2019: Automatic pixel-level multiple damage detection of concrete structure using fully convolutional network. *Computer-Aided Civil and Infrastructure Engineering*, 34, 616-634. doi.org/10.1111/mice.12433.

Markiewicz, J., Tobiasz, A., Kot, P., Muradov, M., Shaw, A., Al-Shamma’a, A., 2019: Review of surveying devices for structural health monitoring of cultural heritage buildings. In: *12th International Conference on Developments in eSystems Engineering (DeSE),* pp. 597-601. IEEE.

Matoušková, E., Kovářová, K., Cihla, M., Hodač, J., 2024: Monitoring biological degradation of historical stone using hyperspectral imaging. *European Journal of Remote Sensing*, 57(1), 2220565.

Nick, W., Asamene, K., Bullock, G., Esterline, A., Sundaresan, M., 2015: A study of machine learning techniques for detecting and classifying structural damage. *International Journal of Machine Learning and Computing*, 5(4), 313.